JOURNAL OF MATERIALS SCIENCE 31 (1996) 1751–1760

Rheological behaviour of a polymer–ceramic blend used for injection moulding

B. LANTERI, H. BURLET
Ecole des Mines de Paris, Centre des Matériaux, BP 87, 91003 Evry Cedex, France
A. POITOU
LMT-ENS Cachan, 21 Av. du Président Wilson, 92000 Cachan, France
I. CAMPION
SNECMA, 291 Avenue d'Argenteuil, 92230 Gennevilliers, France

Our aim is to describe the behaviour of highly filled injection moulding pastes, made of a polymer binder and fine ceramic powders. A specific rheometer has been developed to characterize this behaviour within the injection range of pressures and shear rates. As classical homogeneous models fail to describe the behaviour of the paste, we propose an original model deriving from the mixture theory, taking into account the separate contributions of binder and powder to the global behaviour of the paste. The qualitative and quantitative accuracies of this model are discussed.

1. Introduction

The injection moulding of highly filled blends is used to produce small and low cost complex shapes. This process can be divided into four main stages. First, the ceramic or metallic powders are mixed together with a molten polymeric binder, in order to obtain an homogeneous saturated paste. Second is the forming stage which is similar to the injection moulding of a thermoplastic. Thirdly the debinding stage consists of extracting the binder by dissolving, evaporating, or melting it in order to obtain fragile parts exclusively composed of powder. Finally, sintering confers to the injected parts their final density and mechanical properties.

Several studies [1–5] have shown that numerous problems may arise at every stage of the process. Classical defects are shape distortion, cracks, bubbles or heterogeneities of density at the debinding and sintering stages, but it was evidenced, using mainly X-ray analysis [6] that most of those defects were initiated during the forming stage. It was also shown that the defects could be avoided by controlling the injection parameters, such as the injection pressure, temperature, mould temperature and dimensions of the gates. Fundamentally, the defects arising during the mould filling step seem to have two main causes: (i) the competition between flow and cooling which is also encountered for thermoplastics, and (ii) the heterogeneous nature of the paste, i.e. the ability to dissociate powder and binder and to create powder structures depending on flow conditions and filling rate of the blend.

Our purpose in this paper is to model the injection moulding of highly filled pastes (60 to 70 vol% powder). Usually, the viscosity of these pastes is described using a polymer-like power law, with a relative viscosity depending on the volume fraction of powder. But such models do not take directly into account the contribution of the heterogeneity of the paste to its global behaviour, and do not predict possible powder/binder segregation. Our model is derived from an extension of continuum mechanics, called "mixtures theory", in which each component of the blend brings its own contribution to the global behaviour. We intend to compare the respective performances of the classical method and of our model to the description of the behaviour of the paste.

We will initially describe the experimental procedure used to measure the viscosity of an industrial paste. Then, we will progress to show that the classical model cannot describe the true behaviour of that paste. Our model will then be detailed. We will qualitatively prove its accuracy, and explain the way we quantitatively identify the model's parameters. The results will then be discussed.

2. Experimental details

2.1. Preparation of the suspension

SNECMA uses this paste to manufacture intricate shape foundry cores for superalloy turbine blades. The main components of the binder are a low density poly-ethylene (LDPE)-based plasticizer, which confers on the binder its main rheological characteristics and a fluidizer, which lowers the viscosity, stabilizes the fusion temperature and helps debinding. The binder behaves globally as a Newtonian wax, showing a low fusion temperature ($T_f \approx 50\,^{\circ}C$) and a low viscosity

0022–2461

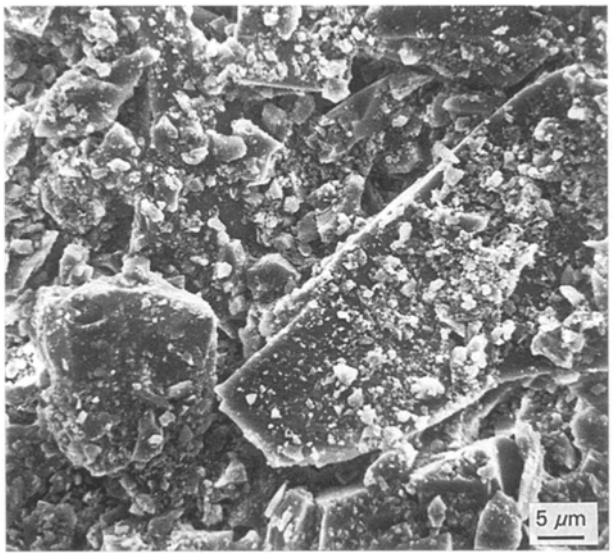

Figure 1 Scanning electron micrograph of the powder.

$\eta_l = 4 \cdot 10^{-2}$ Pa s at the working temperature of 60 °C. The ceramic powder is silica-based, with a large particle size distribution. The particle diameter ranges from 1 to 100 μm, and a scanning electron micrograph of the powder shows sand-like, irregular shaped grains (see Fig. 1).

Various mixture compositions have been prepared with powder loadings in the range 50–70 vol%, in order to detect the critical solids loading ϕ_c. This loading corresponds to the point above which air pockets appear in the blend, as there is not enough binder left to fill all the voids between the particles. ϕ_c is measured by comparing the theoretical densities with experimentally measured ones [7].

Mixing was performed in a small thermally controlled Z-blade apparatus at 100 °C for 90 min. All rheological measurements were carried out on a 60 vol% mixture, which is below the critical volume fraction ϕ_c.

2.2. Viscosity measurements

The capillary rheometer used to measure the viscosity of the paste has been designed, built and tested at Centre des Matériaux [8]. The rheometer has been positioned at the end of an injection moulding machine, whose characteristics are outlined in Table I.

Fig. 2 is a schematic diagram of the rheometer. The capillaries are commercial alumina and stainless steel tubes. The dimensions and nature of the capillaries are reported in Table II. The entire apparatus is thermally regulated at the working temperature of 60 °C. The imposed flow rate in a capillary is deduced from the translation speed of the screw. Two pressure transducers are located at each end of the capillaries to calculate the pressure drop. The end correction to be applied was estimated by using different die lengths and was found to be negligible. Details on the rheometer instrumentation are reported in Table III.

The developed rheometer when attached to an injection moulding machine allows the measurement of

TABLE I Injection moulding machine characteristics

Machine	Allrounder 221-75-350
Screw diameter	22 mm
Screw rotation speed	150 rpm
Screw treated against corrosion	
Maximum pressure	100 MPa

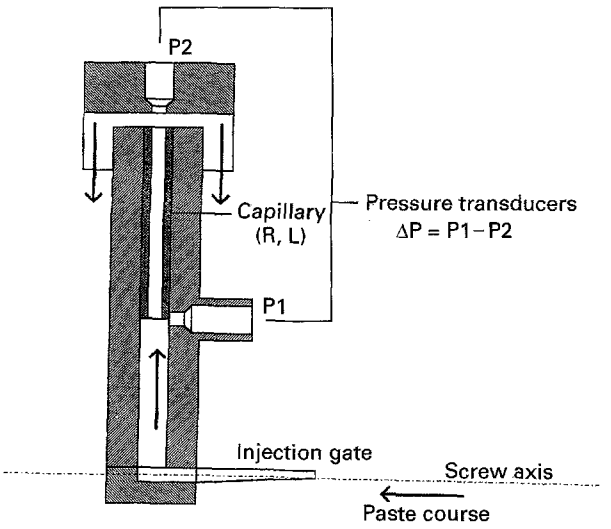

Figure 2 Schematic of the capillary rheometer.

TABLE II Characteristics of the rheometer capillaries

Internal radius R (mm)	Length L (mm)
Alumina capillaries (Desmarquets AF997)	
0.5	140-125-115-70
0.75	140-125-115-70
1.0	140-125-115-70
1.25	140-125-115-70
1.5	140-125-115-70
2.5	115-70
Stainless steel capillaries (Goodfellow AISI 304)	
0.85	140-125-115-75-70
1.15	140-125-115-75-70
2.0	140-125-115-75-70

TABLE III Instrumentation of the capillary rheometer

Flow rate control: LVDT	
Maximum course	50 mm
Resolution	10 μm
Pressure drop measurement: Dynisco PT435A-5M pressure transducer	
Gauge diameter	8 mm
Maximum pressure	100 MPa
Resolution	0.1 MPa
Acquisition	
Machine	PC (80286 microprocessor)
Acquisition card	PC ADDA 12 (Mesurix)
Maximum acquisition speed	760 Acq s^{-1}

the viscosity for a shear rate range close to that of the process condition. Typical values of the pressure drop and shear rate lie in the range:

$$0.1 < \Delta P < 25 \text{ MPa}$$

$$100 < \dot{\gamma} < 10^5 \text{ s}^{-1}$$

The thermal regulation system prevents temperature gradients within the capillary, but viscous dissipation in the paste is still possible for small radii and high shear rates. Temperature measurements at the ends of the capillaries were performed. They show that the temperature rises in capillaries of internal radii below 1 mm, and lengths above 125 mm.

3. Experimental results

The highly filled paste behaviour differs significantly from a single polymer behaviour. A high volume fraction of powder affects the flow of the paste by forming quasi-solid structures which depend mainly on the shear rate, or by the creation of a thin depleted fluid layer at the walls, thus allowing an apparent sliding of the pastes in the dies. Thus all experimental data have to be exhaustively controlled.

The experimentally measured data are the flow rate Q, and the pressure drop ΔP. Typically flow curves relating Q and ΔP for two capillary lengths are drawn in Fig. 3. Each of these curves should be unique since end correction is negligible with this instrumental apparatus. The observed difference is due to experimental dispersion. It is well-known that highly loaded pastes show a greater dispersion than does a thermoplastic (20–30%, instead of 10%). It has been shown that this dispersion is related to the volume fraction, and also to the particle size distribution of powders. The greater the volume fraction and the smaller the size distribution, the larger the dispersion, because the ability of powder grains to reorder themselves decreases when the amount of powder increases, or when the finer particles, playing the role of ball bearings in the flow have been eliminated. Fig. 4 shows a typical time-pressure curve. The stabilized pressure drop is measured after a quite long transient zone, related to the reorganisation of powder networks in the die.

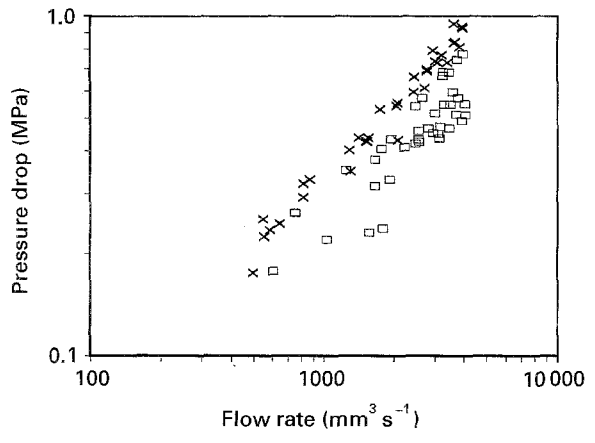

Figure 3 Flow curves for the 60 vol% paste ($R = 2.5$ mm). (×) $L = 115$ mm and (□) $L = 70$ mm.

Due to the cost of the powder, rheometry experiments were conducted with recycled paste. The effect of recycling on the pressure measurements is reported in Fig. 5. With an increasing number of recycles, the dispersion decreases and the pressure drop tends to an asymptotic value. Thermogravimetric analysis and control of the particle size distribution indicate that this decrease is not due to any evolution of the binder or the particles. It probably derives from a micro-homogenization of the blend, since a higher shear rate is developed during the extrusion of the paste in a thin capillary compared to that in the mixing pot, whenever the mixing time is very long.

Analysis of the flow curves is simplified when they are plotted in a diagram relating the shear stress at the wall τ_w versus the apparent shear rate $\dot{\gamma}_a$:

$$\tau_w = \frac{\Delta P \cdot R}{2L} \quad (1)$$

$$\dot{\gamma}_a = \frac{4Q}{\pi R^3} \quad (2)$$

Whatever the die dimensions and the material it is made from, if the paste agrees with the four following

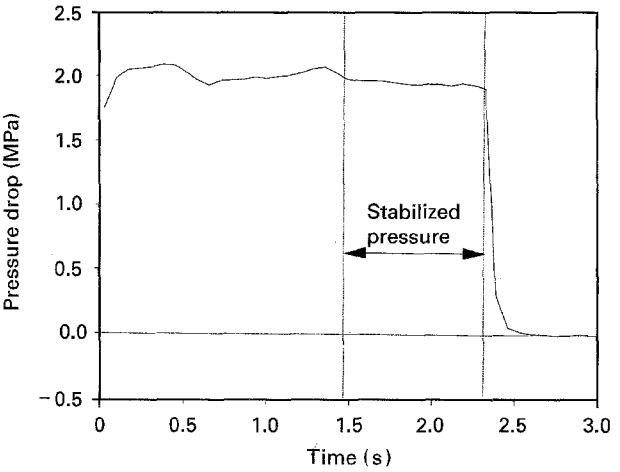

Figure 4 Typical evolution of the pressure drop at the ends of the capillary.

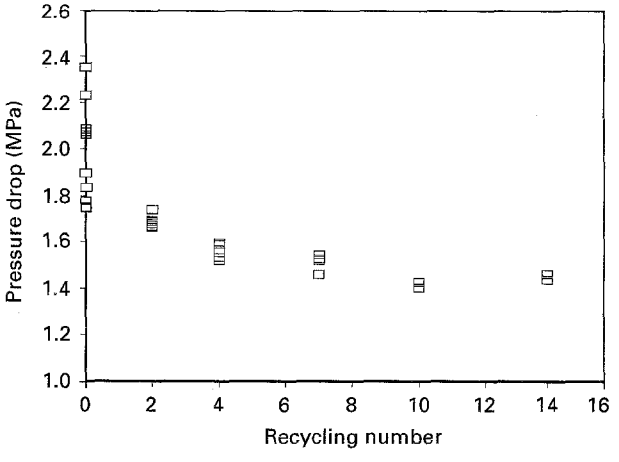

Figure 5 Influence of recycling on the measured pressure drop. $R = 1.5$ mm, $L = 125$ mm, screw speed = 130 mm s^{-1}.

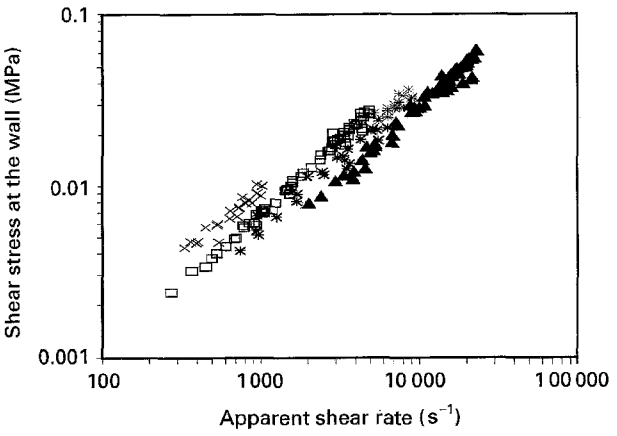

Figure 6 Influence of the tube radius on the flow curves for the 60 vol% paste. (▲) $R = 0.9$ mm, (*) $R = 1.25$ mm, (□) $R = 1.5$ mm and (×) $R = 2.5$ mm.

hypothesis, then there should be only one flow curve, called the "master curve" [9]:

(i) the paste is incompressible;
(ii) its behaviour is time independent;
(iii) the experiments are isothermal;
(iv) the paste sticks at the wall.

It is seen in Fig. 6 that the results obtained with various capillaries lead to separate curves. Hypothesis 1–3 are satisfied, and thus this observation will be analysed in terms of the breakdown of (iv) i.e. the existence of slip at the wall.

4. Discussion

4.1. The apparent slip at the wall

In the following discussion we make the assumption that the geometry dependence is the consequence of wall slipping. The paste is then considered as a homogeneous medium which can be characterized in terms of a power law behaviour. Wall slipping has been observed on many materials and the mechanisms have been investigated. Two main tendencies have been reported in the literature. First, true slippage at the wall, i.e. a real discontinuity of the velocity near the wall, has been observed for unfilled polymers or elastomer blends, but this could also probably be applied to a highly filled blend with a very viscous binder [10, 11]. The sliding law is then similar to solid-like friction laws. Secondly a phenomenon called "apparent slip" has also been observed for polymer solutions, suspensions and filled blends [12–14]. In this case the mechanism is different. Near the wall, the fluid experiences high shear gradients, and thus the powder grains tend to migrate towards the centre of the die. A thin depleted binder layer appears at the surface of the die, and the mean velocity in this layer, in which the viscosity is obviously smaller than the global viscosity of the paste, is assimilated in to the paste velocity at the wall.

Considering the mixture studied in this paper, the binder showed sticky condition and very low viscosity. Thus if slip is present it could only be an apparent slip related to the appearance of a thin depleted film. To date no one has managed to see such a film. We have therefore made the hypothesis that this mechanism is present and have tried to analyse the experimental curves using Mooney's theory [15]. He performed a macroscopic analysis of the slipping phenomenon for fully developed, incompressible, isothermal and laminar flow in circular tubes. He split the measured flow rate Q into a "real" flow rate Q_b, resulting from the global shear of the paste, and a slip flow rate Q_s, depending on the slip velocity V_s. The main hypothesis made by Mooney is that the slip of the paste may be represented as a behaviour law, so that the slip velocity depends only on the shear stress at the wall. The flow rate in the tube may then be expressed as:

$$Q = 2\pi \int_0^R w(r) r \, dr \tag{3}$$

where $w(r)$ is the velocity of the paste in the tube, and R is the die radius. Integration by parts of Equation 3 leads to:

$$Q = [\pi r^2 w(r)]_0^R - \int_0^R \pi r^2 \frac{dw(r)}{dr} dr \tag{4}$$

On the other hand, the shear rate $\dot{\gamma}$ is defined as:

$$\dot{\gamma} = \frac{dw(r)}{dr} = f(\tau) \tag{5}$$

where τ is the shear stress in the paste, with $\tau/r = \tau_w/R$, and f is a function describing the behaviour of the paste. The flow rate Q is then written as a function of τ:

$$Q = Q_s + Q_b = \pi R^2 V_s(\tau_w) + \frac{\pi R^3}{\tau_w^3} \int_0^{\tau_w} f(\tau)\tau^2 \, d\tau \tag{6}$$

By combining Equations (2) and (6), we finally obtain Mooney's formula:

$$\dot{\gamma}_a = \frac{4V_s(\tau_w)}{R} + \frac{4}{\tau_w^3} \int_0^{\tau_w} f(\tau)\tau^2 \, d\tau \tag{7}$$

This formula allows us to evaluate the slip velocity, by plotting the apparent shear rate $\dot{\gamma}_a$ versus the reciprocal of the die radius $(1/R)$ for a given shear stress at the wall τ_w. These curves, (also called Mooney's curves), should be straight lines whose slope is related to the slip velocity. This method has been successfully used by several authors [14, 16]. Mooney's curves are plotted for our material in Fig. 7. We immediately observed that we did not obtain straight lines, but parabolic curves. This infers that Mooney's hypothesis is not applicable to our paste: the slip velocity, defined as the slope of the curves, is dependent on the die radius.

The misfit of Mooney's curve has been previously mentioned in the literature for highly filled pastes [17–20]. Some authors have proposed laws relating V_s, τ_w and the die radius R [21, 22], but these laws are purely empirical, without any theoretical basis. Most of the authors whose results are not compatible with

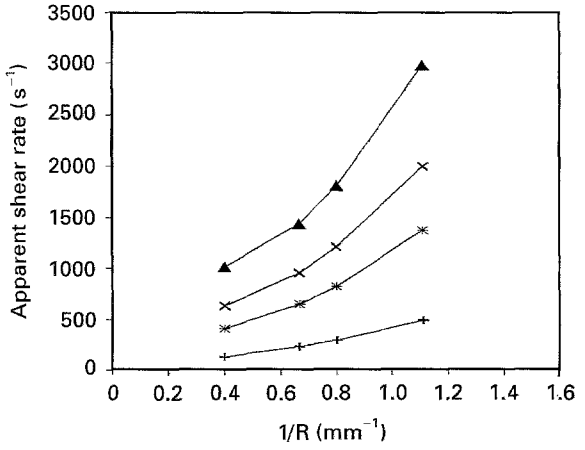

Figure 7 Experimental Mooney's curves for the 60 vol% paste. (▲) 10000 Pa, (×) 7000 Pa, (*) 5000 Pa and (+) 2000 Pa.

Mooney's analysis mention Wiegreffe's analysis, in which he writes:

$$V_s(\tau_w, R) = \frac{\beta(\tau_w)}{4R} \quad (8)$$

where β is called the corrected slip coefficient.

In fact, such expressions fail to represent an intrinsic behaviour law for the paste which is independent of the geometry of the considered die. A solution may consist in experimentally investigating another shear-rate range, or in modifying the surface conditions at the wall, thus defining a sticking zone within which it would be possible to identify the real behaviour of the paste and thus to isolate the second term of Equation 7 [20]. Unfortunately the accurate experimental conditions necessary to perform such an analysis, these include several rheometers and optimal control of internal die surfaces, especially those of the capillaries, were not available in our case.

We have simply proven that the rheological behaviour of this mixture can not be described by considering the paste as a homogeneous medium with slipping condition. We now propose to analyse the observed flow curves considering the heterogeneous nature of the paste.

4.2. Analysis of the heterogeneous behaviour of the paste

The theory of mixtures is an extension of continuum mechanics. This study is inspired by the works of Poitou on extrusion [23]. In this paper, we discuss the application of the theory of mixtures to the description of the flow of two different components. The chosen components are the wax binder and the lubricated powder. Each component is defined by its velocity $\vec{v}_i$ by its volume fraction α_i ($i = l$ or p), and by its behaviour and boundary conditions. These last assumptions impose the limitation that the solid volume fraction is high enough to consider the powder particles as a continuous medium, characterized by constitutive equations. The corresponding minimum volume fraction ϕ_{min} is determined from measurements of the shrinkage on debinded parts. The curve showing the evolution of the measured shrinkage versus the binder volume fraction slowly increases up to ϕ_{min} and abruptly increases beyond this value. Experiments gave $\phi_{min} = 57$ vol%. This model is developed under the assumption that each component is incompressible. Unfortunately, air cannot be treated in this approach, and the model cannot thus be applied to unsaturated blends. In turn, this means that the filling rate must be less than a critical volume fraction ϕ_c, which has been experimentally determined to be around 70 vol%. Finally, all the following equations should be applied within a given range of filler volume fraction $\phi_{min} < \phi < \phi_c$.

4.2.1. Mass conservation

The mass balance for constituent i is written as follows:

$$\frac{d}{dt}\int_V \rho_i \, dv = \int_V c_i^* \, dv \quad (9)$$

where ρ_i is the apparent density of constituent i, and the mass supply c_i^* represents the mass exchange with the other constituent. Since no chemical reaction occurs between the ceramic powder and the polymeric binder during the filling stage, it is possible to write that $c_i^* = 0$. After suitable manipulation, the local form of Equation 9 is extracted:

$$\frac{\partial \rho_i}{\partial t} + \mathrm{div}(\rho_i \vec{v}_i) = 0 \quad \text{with} \quad \rho_i = \alpha_i \gamma_i$$

where γ_i is the material density of constituent i, which represents the mass of this constituent per unit volume. The ceramic powder and the wax binder are assumed to be incompressible ($d\gamma_i/dt = 0$), thus the mass balance reduces to:

$$\frac{\partial \alpha_i}{\partial t} + \mathrm{div}(\alpha_i \vec{v}_i) = 0 \quad (10)$$

Additionally, the volume fractions α_i have to verify:

$$\sum_{i=1}^{n} \alpha_i = 0 \quad \text{and} \quad \sum_{i=1}^{n} \frac{\partial \alpha_i}{dt} = 0$$

A new equation, characterizing the global incompressibility of the paste, may then be deduced from the sum of the mass conservations:

$$\mathrm{div}(\alpha_l \vec{v}_l + \alpha_p \vec{v}_p) = 0 \quad (11)$$

where $\alpha_l \vec{v}_l + \alpha_p \vec{v}_p$ is defined as the mean velocity of the paste. Note that, due to the global incompressibility of the blend, $\vec{v}_l = \vec{v}_p$ leads to $\mathrm{div}(\vec{v}_l) = \mathrm{div}(\vec{v}_p) = 0$, and from Equation 10 to $\dot{\alpha}_e = \dot{\alpha}_p = 0$. This means that the composition of the blend will change only if there is a relative movement between the two constituents.

4.2.2. Balance of momentum

The balance of linear momentum for each constituent is:

$$\frac{d}{dt}\int_V \rho_i \bar{v}_i dv + \int_S \bar{T}_i ds = \int_V \rho_i \bar{b}_i dv + \int_V \bar{p}_i^* dv \quad (12)$$

where $\bar{T}_i = \overline{\overline{\sigma_i}} \cdot \bar{n}$ is the flux vector representing the efforts transmitted through the surface S, $\bar{b}_i$ is the external body force exerted on volume V_i (i.e. gravity, centrifugal forces, ...), and the momentum supply $\bar{p}_i^*$ results from drag forces due to the presence and motion of the other contituents. The local form of the linear momentum is the partial equilibrium of the constituent and is obtained from Equation 12:

$$\rho_i \frac{d\bar{v}_i}{dt} = \overline{\mathrm{div}}(\overline{\overline{\sigma_i}}) + \rho_i \bar{b}_i + \bar{p}_i^* \quad (13)$$

For a wax binder and a silica-based powder, with a 60 vol% powder fraction, the global viscosity of the paste is above 10 Pa s, and the powder density is $\rho_p = 2.44\ \mathrm{g\,cm^{-3}}$. Inertia and gravity terms may then be neglected. Equation 13 reduces to a simple Stoke's form:

$$\overline{\mathrm{div}}(\overline{\overline{\sigma_i}}) = -\bar{p}_i^* \quad (14)$$

As the considered flow is isothermal, it is not useful to write the conservations of energy and entropy.

4.2.3. Constitutive laws and boundary conditions

The main hypothesis on the constituents behaviour is that each partial stress depends exclusively on the velocity of the associated constituent. If this assumption were not made, then the identification of the material parameters would be impossible. A pseudo-plastic fluid behaviour has then been associated to both constituents:

$$\overline{\overline{\sigma_i}} = -\alpha_i p \overline{\overline{I}} + 2\eta_i \tilde{\dot{\varepsilon}}_i^{(m_i-1)} \overline{\overline{\dot{\varepsilon}_i}} \quad \text{with}$$

$$\tilde{\dot{\varepsilon}}_i = (2Tr(\overline{\overline{\dot{\varepsilon}_i}} : \overline{\overline{\dot{\varepsilon}_i}}))^{1/2} \quad (15)$$

where η_i is the consistency of the component, m_i is its melt flow index. $\tilde{\dot{\varepsilon}}_i$ is the generalized shear rate for the constituent. In the present study, the binder shows a Newtonian behaviour, so that $m_b = 1$ and $m_p = m$.

According to the binder's fluidity, it seems reasonable to let it stick at the wall:

$$\bar{v}_l = \bar{0} \quad (16)$$

The lubricated powder may also stick at the wall, but the flow of highly filled pastes in moulds or dies sometimes evidences wall effects, such as apparent slip at the wall. That slip is commonly related to the appearance at the surface of the blend of a thin depleted fluid layer, due to particle migration towards the centre of the die [14, 19]. The slipping law associated to the lubricated powder is:

$$\tau_p = -f_p(v_p^t - w^t) \quad (17)$$

where τ_p is the shear stress at the wall, f_p is the friction coefficient, w^t is the tangential velocity of the wall (usually, $w^t = 0$), and v_p^t is the tangential velocity of the powder. The condition of non-penetration yields:

$$\bar{v}_p \cdot \bar{n} = \bar{w} \cdot \bar{n} \quad (18)$$

where $\bar{n}$ is the outside normal vector on the wall.

On the free surface at the outlet of the mould, the boundary condition on both constituents describes a local equilibrium with the outer medium:

$$p_p + p_b = p_{\mathrm{atm}} \quad (19)$$

where p_b and p_p are the partial pressures associated to the constituents, and p_{atm} is the atmospheric pressure.

Although more general forms have been proposed [24–26], the authors who have tried to relate those equations to experiments generally admitted that the momentum supply was as equally well described by Darcy's law [27, 28]:

$$\bar{p}_p^* = -\bar{p}_b^* = k(\bar{v}_b - \bar{v}_p) \quad (20)$$

where k is the interaction coefficient relating the powder and the binder. According to Darcy's law, k is the ratio of the fluid viscosity to the powder bed permeability β. In this model, k will be considered constant, and identified *a posteriori*, from rheological tests on the paste, but the former definition suggests a dependence of k on the powder volume fraction, through the permeability term.

4.2.4. General equations

The unknowns of the problem are the velocities $\bar{v}_l$ and $\bar{v}_p$, and the volume fractions α_l and α_p of the defined constituents: the binder alone, and the lubricated powder. Substituting in Equation 14 the partial stresses and the momentum supply with their expressions given in Equation 15 and Equation 20 yields:

$$\alpha_b \overline{\mathrm{grad}}\, p + \overline{\mathrm{div}}(2\eta_b \overline{\overline{\dot{\varepsilon}_b}}) = -k(\bar{v}_b - \bar{v}_p) \quad (21)$$

$$\alpha_p \overline{\mathrm{grad}}\, p + \overline{\mathrm{div}}(2\eta_p \tilde{\dot{\varepsilon}}_p^{(m-1)} \overline{\overline{\dot{\varepsilon}_b}}) = k(\bar{v}_b - \bar{v}_p) \quad (22)$$

We will from now on consider the particular case of laminar stationary flows in rheometer dies. For both constituents, apart from their relative motion, the flow lines are straight and parallel to the axis of the flow, which leads to $\mathrm{div}(\bar{v}_l) = \mathrm{div}(\bar{v}_p) = 0$. The mass balance, Equation 10, is then naturally satisfied, and there will be no evolution in the composition of the blend for those flows. The remaining equations for the model are Equation 21 and Equation 22, together with Equation 11, the boundary conditions being described by Equations 16–19.

4.3. Analysis of the apparent slip at the walls using a reduced model

Our objective is to analyse the laminar stationary flow of a heterogeneous paste in a preselected geometry, e.g. a capillary of radius R and length L. Consideration

of the reduced equations for the model, written for two Newtonian constituents both sticking at the walls of the die, allows us to discuss analytic expressions. In this case, the solution of the movement equations is expressed in terms of the Bessel function I_0:

$$v_l(r) = \frac{\Delta P}{4L(\eta_l + \eta_p)} \cdot (R^2 - r^2) + \frac{\Delta P}{\omega^2 L} \times \left(\frac{1}{\eta_l + \eta_p} - \frac{\alpha_l}{\eta_l}\right) \cdot \left(\frac{I_0(\omega r)}{I_0(\omega R)} - 1\right) \quad (23a)$$

$$v_p(r) = \frac{\Delta P}{4L(\eta_l + \eta_p)} \cdot (R^2 - r^2) + \frac{\Delta P}{\omega^2 L} \times \left(\frac{1}{\eta_l + \eta_p} - \frac{\alpha_p}{\eta_p}\right) \cdot \left(\frac{I_0(\omega r)}{I_0(\omega R)} - 1\right) \quad (23b)$$

$$\text{where} \quad \omega = \left(\frac{k(\eta_l + \eta_p)}{\eta_l \eta_p}\right)^{1/2}$$

$$\text{and} \quad I_0(\omega r) = \sum_{n=0}^{\infty} \frac{(\omega r)^{2n}}{2^{2n} n!(n+1)!}$$

Note that ω only depends on the material characteristics.

The volume flow rate in the capillary is defined in terms of the mean velocity of the paste:

$$Q = \int_0^R 2\pi r \{\alpha_l v_l(r) + \alpha_p v_p(r)\} \, dr \quad (24)$$

Using Equations 23a and 23b, and after some rearrangement, Equation 24 becomes:

$$Q = \frac{\Delta P \pi R^4}{8L(\eta_l + \eta_p)} + \frac{2\pi \Delta P R}{L\omega^3} \cdot \left(\frac{I_1(\omega R)}{I_0(\omega R)} - \frac{\omega R}{2}\right) \times \left(\frac{1}{\eta_l + \eta_p} - \frac{\alpha_p^2}{\eta_p} - \frac{\alpha_l^2}{\eta_l}\right)$$

$$\text{where} \quad I_1(\omega r) = \sum_{n=0}^{\infty} \frac{(\omega r)^{1+2n}}{2^{(1+2n)} n!(n+2)!} \quad (25)$$

This equation may be written in a more manageable form by introducing an effective viscosity of the mixture η^*, defined as $\eta^* = \eta_l + \eta_p$.

The combination of Equation 25, with Equation 1 and Equation 2 leads to an expression of the apparent shear rate function of the shear stress at the wall τ_w and of the tube radius R which is analogous to Mooney's formula:

$$\dot{\gamma}_a = \frac{\tau_w}{\eta^*} + \frac{16\tau_w}{\omega^3 R^3} \cdot \left(\frac{I_1(\omega R)}{I_0(\omega R)} - \frac{\omega R}{2}\right) \cdot \left(\frac{1}{\eta^*} - \frac{\alpha_p^2}{\eta_p} - \frac{\alpha_l^2}{\eta_l}\right) \quad (26)$$

The first term on the right-hand side of this equation describes the behaviour of a homogeneous Newtonian sticking fluid in which the viscosity is the effective viscosity η^*. The second term of the equation derives from the heterogeneity of the paste, and shows that the flow curves deduced from this model depends explicitly on the die radius R, for a given set of constituent characteristics. This equation has obviously the same form as Mooney's formula, Equation 7, with an extra geometric dependency.

While ω is a dimensionless term, containing exclusively the characteristic parameters of the material, we may plot the apparent fluidity $(\dot{\gamma}_a/\tau_w)$ against $(1/\omega R)$ as a master Mooney's curve (see Fig. 8).

Reasonable values for ω lie in the range $10^{-2} < \omega < 10^4$, and this curve exhibits three distinct zones:

(i) low values of ωR ($\omega R < 1$) are nonsensical values.

(ii) Higher ωR values correspond to a polynomial quadratic curve for the second term of the equation, which means that for a given mixture (i.e. for a given ω), the apparent shear rate depends on $(1/R^2)$ at a given τ_w. This result is very interesting, because it leads to a late justification of Wiegreffe's analysis (see Equation 8 [18, 19, 22]). Note that this dependency is not the consequence of a discontinuity in the velocity at the interface between the material and the mould, but is due to a relative motion of the two phases.

(iii) As ωR becomes large, the first term of Equation 26 becomes predominant, and we find a Newtonian fluidity. The material may then be considered homogeneous, due either to a high value of the tube radius, the interaction coefficient k, or of the (η_p/η_l) ratio.

The previous conclusions are very important since they mean that within a given range of capillary size, the behaviour of a mixture may be described using a classical polymer law. This assessment should now be verified with other types of flows, such as flow through plates. The solution of the movement equations is, for a flow through a plate of height h:

$$\dot{\gamma}_a = \frac{\tau_w}{\eta^*} - \frac{12\tau_w}{\omega^2 h^2} \cdot \left(\frac{1}{\eta^*} - \frac{\alpha_p^2}{\eta_p} - \frac{\alpha_l^2}{\eta_l}\right) \quad (27)$$

Fig. 9 shows these two analogous equations, involving the same invariants for the material η^*, ω and $(1/\eta^* - \alpha_p^2/\eta_p - \alpha_l^2/\eta_l)$. Both curves have the same shape:

(i) a zone for high values of ωR (or ωh), in which the mixture behaves as a homogeneous polymer, with an effective viscosity η^*,

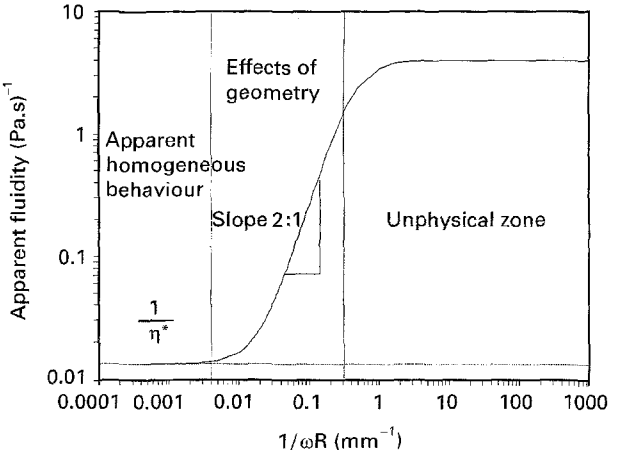

Figure 8 Simulated fluidity curve for a heterogeneous Newtonian paste.

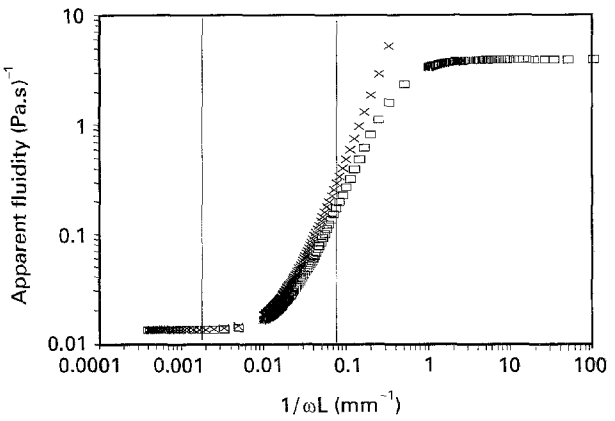

Figure 9 Simulated fluidity curves for (□) capillaries and (×) plates.

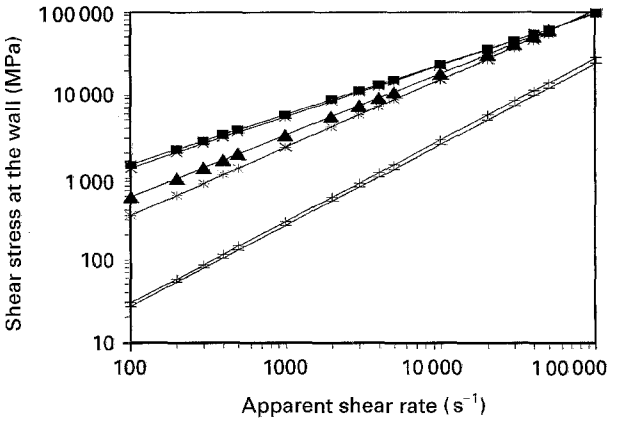

Figure 10 Simulated flow curves for a heterogeneous pseudoplastic paste for flows of: (−) $R = 0.05$ mm, (+) $R = 0.1$ mm, (*) $R = 1$ mm, (▲) $R = 5$ mm, (×) $R = 10$ mm and (■) $R = 50$ mm.

(ii) a zone of lower ωR (or ωh), in which the apparent shear rate depends on the geometry of the die. It is worth noting that the transition arises for the same range of R and h. Thus, this simplified form of the model may be applied in every mould geometry having the same thickness.

Equations 23a, b–27 have been derived in the case of two Newtonian constituents. However, injection blends usually show a pseudoplastic behaviour. Unfortunately for the present theory, global pseudoplasticity cannot be obtained with Newtonian constituents. This model then requires a non-Newtonian law for the particle behaviour. The corresponding equations have no analytical solutions. Therefore, the model has been implemented into a finite element code in order to predict the behaviour of more sophisticated mixtures. Calculations have been performed with a Newtonian fluid ($\eta_l = 0.04$ Pa s) and a pseudoplastic lubricated powder ($\eta_p = 75$ Pa s, $m = 0.75$), related by a low interaction term ($k = 5$ Pa s mm^{-2}). The chosen geometries were capillaries, with various radii R. We plot in Fig. 10 the global flow curves giving τ_w against $\dot{\gamma}_a$ for the different geometries. Once again, we see distinct flow curves, showing a power-law behaviour. We note that the slope of these curves, and consequently the global melt flow index $\bar{m}$ of the mixture also depends on the die radius, with $m < \bar{m} < 1$. Obviously, such curves cannot be analysed through Mooney nor Wiegreffe's theories. In order to make an analogy with the previous results, we plot the apparent fluidity curves $\dot{\gamma}_a/(\tau_w)^{(1/m)}$ against $1/\omega R$ in Fig. 11. Each one corresponds to a given wall shear stress. We observe the same three zones obtained with the reduced expression, Equation 26, and it seems that Mooney's formula should be expressed in the following way:

$$\dot{\gamma}_a = \frac{4m}{3m+1}\left(\frac{\tau_w}{\eta^*}\right)^{1/m} + h\left(\tau_w, m, \{\omega R\}, \times\left\{\frac{1}{\eta^*} - \frac{\alpha_p^2}{\eta_p} - \frac{\alpha_l^2}{\eta_l}\right\}\right) \quad (28)$$

where we again find the first homogeneous term, and also a second polynomial term depending on the heterogeneous invariants.

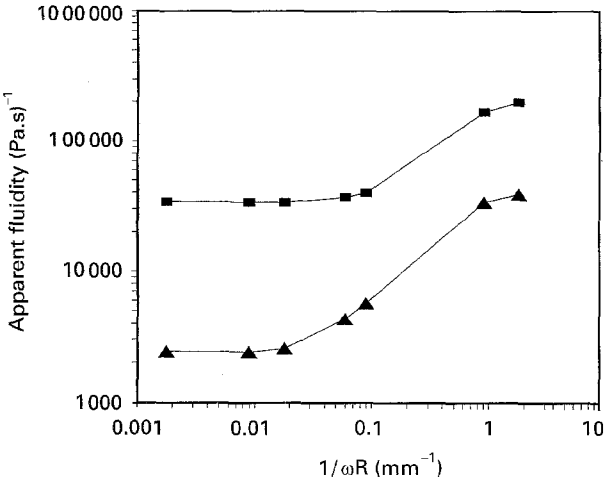

Figure 11 Simulated fluidity curves for a heterogeneous pseudoplastic paste. (■) 50 000 Pa and (▲) 10 000 Pa.

The conclusions of this analysis are, first, that this model makes it possible to take into account the effect of the die radius on the behaviour of the pastes, by considering exclusively the volumetric separation of the binder and of the powder, apart from all slipping effects. Conversely, the knowledge of the material parameters for our model allows us to predict whether the dependence on the mould geometry will be determinant during the flow of the paste. Finally, because we cannot extract the analytical expressions for a pseudoplastic blend, a finite element tool was required to predict the global behaviour of the paste. This tool allows us to identify the model's parameters.

4.4. Identification process for the heterogeneous parameters

The present model requires the determination of four material parameters: η_l, η_p, m and k. They have been identified from the experimental results presented in Section 2. Some of the parameters have been fixed. The viscosity η_l of the binder in the mixture has been taken to be equal to the viscosity of the binder itself, which was known from Couette measurements

(see Section 2.1). On the other hand, the dispersion of the rheometric measurements on the paste do no allow us to estimate precisely the variation of the global melt flow index $\bar{m}$ as a function of the die radius (see Fig. 6). Hence, we assumed that $\bar{m} = m \approx 0.75$. Eventually, we only need to fit the lubricated powder consistency η_p, and the interaction coefficient k.

The identification process is represented in Fig. 12. The finite element code allows us to simulate the flow of the heterogeneous blend in several tubes of known radius and length. For a given flow rate, the code estimates the global pressure drop at the ends of the tube. The simulated flow curves τ_w against $\dot{\gamma}_a$ and Mooney's curves $\dot{\gamma}_a$ against $(1/R)$ are then plotted against the corresponding experimental curves, and the unknown parameters are adjusted to fit the experiments.

The best agreement was obtained with the following set of heterogeneous parameters:

$$\eta_l = 0.04\ \text{Pa s}, \quad \eta_p = 75\ \text{Pa s}, \quad m = 0.75$$

$$k = 5\ \text{Pa s mm}^{-2}$$

Experimental data and numerical simulation are compared in Fig. 13. We note that the interaction coefficient k is very low, and that, due to the very low binder viscosity, the lubricated powder characteristics are close to the global blend characteristics. Once the parameters have been identified from a set of capillary experiments, we must validate this approach on other experiments.

4.5. Validation of the model

The validation consists of an injection at a fixed flow rate in an instrumented axisymmetric plate (see Fig. 14). A technique called "volume control" is used to simulate the filling of the mould. Note that the solid volume fraction is set constant and equal to its initial value. Further details can be found in references [29] and [30]. Numerical and experimental data are compared in terms of the evolution of the pressure drop between the transducers set at $R = 10$ mm and $R = 20$ mm against time (see Fig. 15). The calculated data obviously do not fit the experimental data, although the scale of pressures is convenient. Since the mean value of the pressure drop is very sensitive to the interaction coefficient, we found that a good agreement could be obtained for a higher interaction coefficient of 15 Pa s mm^{-2} (instead of 5 Pa s mm^{-2}). But this value does not fit the capillary results. The failure of the model to fit both experiments indicates that the model is not sophisticated enough. We suspect the interference of wall effects, since the axisymmetric mould is made of aluminium, while the rheometer capillaries are made of alumina. Hence, we carried out further rheometric experiments, using untreated stainless steel capillaries. The Mooney's curves obtained for stainless steel and alumina capillaries are

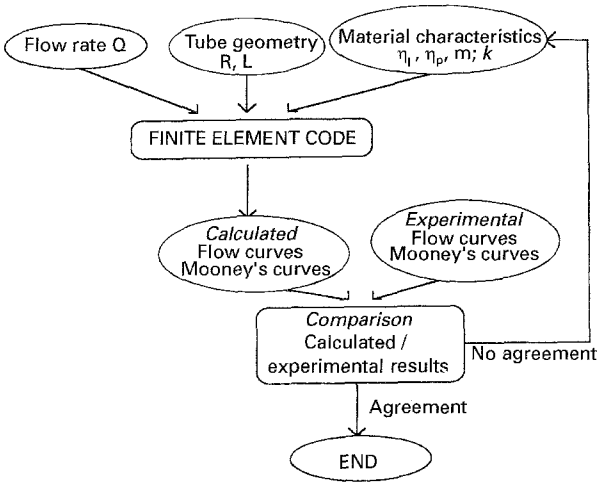

Figure 12 Identification process of the model parameters η_p and k.

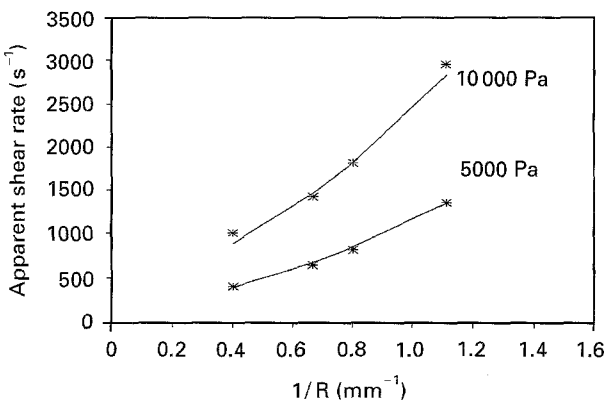

Figure 13 (−) Simulated and (∗) experimental Mooney's curves for the 60 vol% paste.

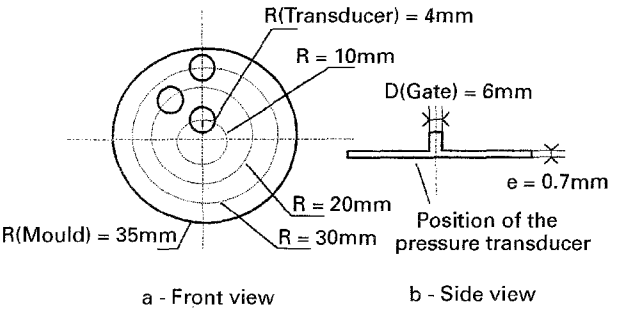

Figure 14 Scheme of the axisymmetric instrumented mould.

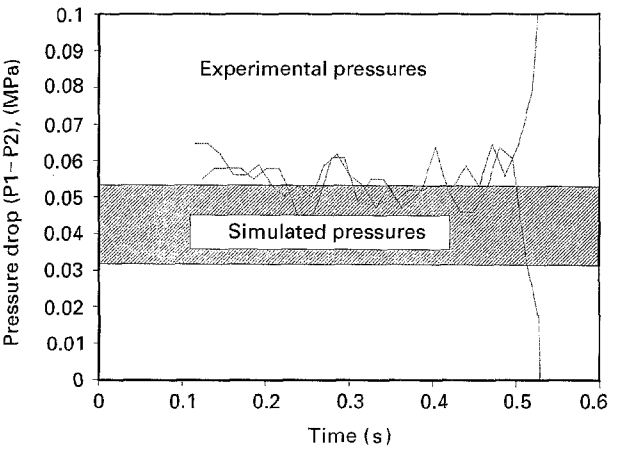

Figure 15 Experimental and simulated pressure drop in the axisymmetric plate.

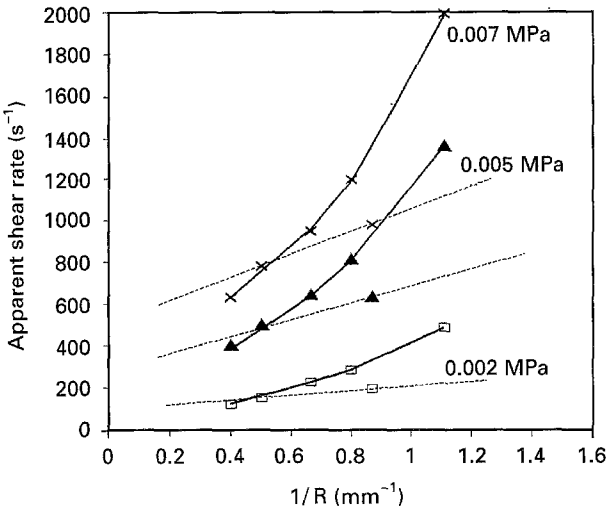

Figure 16 Mooney's curves for (---) stainless steel and (——) alumina capillaries.

represented on Fig. 16. The mismatch of the two sets of curves suggest that the global behaviour of the paste includes wall effects in addition to powder binder relative movement. Further developments of the model should take into account friction laws.

5. Conclusions

Rheological measurements have been performed on highly loaded polymers. Several diameters have been used in order to analyse slip problems. The range of the selected geometries is quite large. Apparent slip at the wall was observed, and a Mooney's analysis indicated a slip velocity depending on both wall shear stress and die radius. This last dependancy is very disturbing since a friction law could not depend on geometric factors. Thus the rheological behaviour of such blends cannot be described like a homogeneous medium with a friction law.

A heterogeneous model has been derived from the mixture theory. The main assumption is that each component is characterized through its own volume fraction, velocity, constitutive equation, and boundary conditions. A momentum supply is introduced to take into account the interaction of the binder with the powder. The simplest form of this supply is a Darcy's law. Extensive analysis of this model showed that the simulated flow curves, obtained with both constituents sticking at the wall, depend on the die geometry, with a dependency different from a Mooney's dependency. Much more interesting is that this dependency is similar to a Wiegreffe's model based on a slip velocity depending on $(1/R)$.

The proposed model has been tested on an industrial paste. The coefficients were determined using a finite element code. A set of parameters were found, and a good agreement was observed between numerical simulations and experimental data. A last validation was then performed. Pressure drop measurements have been done during the filling of an axisymmetric disk. A mismatch was observed between the prediction of the model and the experimental data. It suggests that the proposed model is not sophisticated enough. In particular, a friction law for the powder constituent is not yet introduced into the model. This development should be guided by other accurate rheological measurements.

Acknowledgement

The authors wish to thank SNECMA for the financial support of this work.

References

1. J. G. ZHANG, M. J. EDIRISINGHE and J. R. G. EVANS, *Ind. Ceram.* **9** (1989) 72.
2. K. N. HUNT, J. R. G. EVANS and J. WOODTHORPE, *J. Mater. Sci.* **26** (1991) 285, 2143, 5229.
3. N. PICCIRILLO and D. LEE, *Int. Jnl. Powder Metall.* **28** (1992) 13.
4. K. F. HENS, D. LEE and R. M. GERMAN, *ibid.* **27** (1991) 141.
5. M. J. EDIRISINGHE and J. R. G. EVANS, *Mat. Sci. Eng.* **A109** (1989) 17.
6. *Idem., J. Mater. Sci.* **22** (1987) 2267.
7. R. M. GERMAN, "Powder Injection Molding" (MPIF, Princeton, New Jersey, 1990).
8. M. DUBUS, "Etude de l'injection de pâtes très chargées", Thèse Conservatoire National des Arts et Métiers (1994).
9. A. WEILL, *Techniques de l'Ingénieur* **A3615**, 1.
10. J. L. WHITE, M. H. HAN, N. NAKAJIMA and R. BRZOSKOWSKI, *J. Rheol.* **35** (1991) 167.
11. N. EL KISSI and J. M. PIAU, *J. Non-Newt. Fluid Mech.* **37** (1990) 55.
12. Y. COHEN and A. B. METZNER, *J. Rheol.* **29** (1985) 67.
13. H. MÜLLER-MOHNSSEN, D. WEISS and A. TIPPE, *ibid.* **34** (1990) 223.
14. U. YILMAZER and D. M. KALYON, *ibid.* **33** (1989) 1197.
15. M. MOONEY, *ibid.* **2** (1931) 210.
16. A. YOSHIMURA and R. K. PRUD'HOMME, *ibid.* **32** (1988) 53.
17. Z. D. JASTRZEBSKI, *Ing. Eng. Chem. Fund.* **6** (1967) 445.
18. W. KOZICKI, S. N. PASARI, A. R. K. RAO and C. TIU, *Chem. Eng. Sci.* **25** (1970) 41.
19. J. L. KOKINI and M. DERVISOGLU, *J. Food Eng.* **11** (1990) 29.
20. P. MOURNIAC, J. F. AGASSANT and B. VERGNES, *Rheologica Acta* **31** (1992) 565.
21. K. GEIGER, *Kautschuk + Gummi Kunstoffe* **42** (1989) 273.
22. S. WIEGREFFE, *ibid.* **44** (1991) 216.
23. A. POITOU, "Approche Mécanique du Mélange par Extrusion", Thèse Ecole des Mines de Paris (1988).
24. R. M. BOWEN, R. A. GROT and G. A. MAUGIN, Continuum Physics, III: "Mixtures and EM Field Theories", C. Eringen Ed. (Academic Press, 1976).
25. A. BEDFORD and D. S. DRUMHELLER, *Int. J. Eng. Sci.* **21** (1983) 863.
26. J. W. NUNZIATO, "Theory of Dispersed Multiphase Flow", R. E. Meyer Ed. (Academic Press, 1983).
27. W. D. BENNON and F. P. INCROPERA, *Int. J. Heat Mass Transfer* **30** (1987) 2161.
28. S. GANESAN and D. R. POIRIER, *Met. Trans.* **21B** (1990) 173.
29. B. LANTÉRI, "Etude du Comportement Rhéologique d'un Mélange Polymère-Céramique destiné à l'Injection", Thèse Ecole des Mines de Paris (1993).
30. B. LANTÉRI, H. BURLET, A. POITOU and N. BURKHARTH, "Mathematical Modelling for Materials Processing", edited by M. Cross, J. F. T. Pittman and R. D. Wood (Clarendon Press, Oxford, 1993) p. 339.

Received 2 September 1994
Accepted 8 September 1995